Thesis for the degree of Licentiate of Engineering

Approaches to particle acceleration in intense laser-matter interaction

Joel Magnusson

Department of Physics
Chalmers University of Technology
Gothenburg, Sweden, 2018

Approaches to particle acceleration in intense laser-matter interaction
Joel Magnusson

Department of Physics
Chalmers University of Technology
SE–412 96 Gothenburg
Sweden
Telephone +46 (0)31-772 1000

Cover:
A 2D particle-in-cell simulation of chirped-standing-wave acceleration. A chirped laser pulse (blue) is normally incident on a thin foil of electrons (green) and protons (red), placed half a wavelength away from a mirror consisting of electrons and ions (grey). The left figure shows the main acceleration stage of the protons in the simulated coordinate space, while the right shows the time evolution of a 1D cut-out along the laser propagation axis.

Chalmers Reproservice
Gothenburg, Sweden, 2018

Approaches to particle acceleration in intense laser-matter interaction
JOEL MAGNUSSON
Department of Physics
Chalmers University of Technology

Abstract

In the interaction of ultra-intense laser fields with matter, the target is rapidly ionized and a plasma is formed. The ability of a plasma to sustain acceleration gradients, orders of magnitude larger than achievable with conventional accelerators, has led to a great interest in laser-driven plasma-based particle acceleration and radiation generation, with applications in materials science, biology and medicine.

In this thesis we consider laser-driven plasma-based particle acceleration by studying the interaction of intense laser fields with solid density targets. The basics of such interactions are described and some of the most common acceleration schemes are presented. We study the effect of adding microstructures on the illuminated side of a solid target and show how this affects the resulting distribution of hot electrons.

Furthermore, we discuss how to achieve controllable ion acceleration through displacement of electrons by standing waves. A recently proposed laser-driven ion acceleration scheme, called chirped-standing-wave acceleration, is introduced and described in detail. Finally, we analyze the robustness of this acceleration scheme under non-ideal conditions and discuss its prospects and limitations.

Keywords: plasma, laser, nonlinear dynamics, laser-matter interaction, particle acceleration, particle-in-cell

Publications

This thesis is based on the following publications:

[I] **Energy partitioning and electron momentum distributions in intense laser-solid interactions**
J. Magnusson, A. Gonoskov, M. Marklund
Eur. Phys. J. D **71**, 231 (2017).
https://doi.org/10.1140/epjd/e2017-80228-1

[II] **Prospects for laser-driven ion acceleration through controlled displacement of electrons by standing waves**
J. Magnusson, F. Mackenroth, M. Marklund, A. Gonoskov
arXiv:1801.06394.
https://arxiv.org/abs/1801.06394

Other publications by the author that are not included in the thesis:

- **Nano and micro structured targets to modulate the spatial profile of laser driven proton beams**
  L. Giuffrida, K. Svensson, J. Psikal, D. Margarone, P. Lutoslawski, V. Scuderi, G. Milluzzo, J. Kaufman, T. Wiste, M. Dalui, H. Ekerfelt, I. Gallardo Gonzalez, O. Lundh, A. Persson, A. Picciotto, M. Crivellari, A. Bagolini, P. Bellutti, J. Magnusson, A. Gonoskov, L. Klimsa, J. Kopecek, T. Lastovicka, G.A.P. Cirrone, C.-G. Wahlström, G. Korn
  J. Instrum. **12**, C03040 (2017).
  http://stacks.iop.org/1748-0221/12/i=03/a=C03040

- **Manipulation of laser-accelerated proton beam profiles by nanostructured and microstructured targets**
  L. Giuffrida, K. Svensson, J. Psikal, M. Dalui, H. Ekerfelt, I. Gallardo Gonzalez, O. Lundh, A. Persson, P. Lutoslawski, V. Scuderi, J. Kaufman, T. Wiste, T. Lastovicka, A. Picciotto, A. Bagolini, M. Crivellari, P. Bellutti, G. Milluzzo, G. A. P. Cirrone, J. Magnusson, A. Gonoskov, G. Korn, C.-G. Wahlström, D.Margarone
  Phys. Rev. Accel. Beams **20**, 081301 (2017).
  https://doi.org/10.1103/PhysRevAccelBeams.20.081301

Contents

Acknowledgments

I would first and foremost like to express my deepest gratitude towards my supervisors Arkady Gonoskov and Mattias Marklund for all of their support, and for continuing to both inspire and encourage me. I would also like to thank Andreas Isacsson for his guidance, as well as for sharing his wisdom whenever I disturb him in his office. I am grateful to my many colleagues and especially past and present members of my research group with whom I have had many laughs, and for creating a pleasant and comradely environment. A special thanks to my office mate Tom for continuing to put up with me and to Benjamin for making sure our office sofa is never alone. Finally I would like to express my gratitude to my family and friends for their support and for giving me so many reasons to smile.

Joel Magnusson, 2018

Chapter 1

Introduction

The topic of this thesis is the analysis of particle acceleration in the interaction of intense laser fields with matter. It will mainly focus on describing the concept of *chirped-standing-wave acceleration* (CSWA), as a means for controllable ion acceleration. Moreover, it will also give a brief overview of laser-matter interaction in general, focusing on how energy can be transferred from the laser to the particles and mentioning a couple of the most commonly studied acceleration schemes.

Since the advent of the first functioning laser in the year 1960 [1], the capabilities of lasers have been greatly improved. The research on the interaction between strong laser fields and matter first began in the 1970s, largely focusing on the topic of atomic physics as well as laser-induced nuclear fusion. The maximum achievable laser intensities however stagnated at relatively moderate levels as it was still intense enough to damage the gain medium, thereby becoming limited by the size of the lasing crystals. It was not until after the invention of *chirped-pulse amplification* (CPA) [2] in 1985 that this limitation was truly overcome and lasers have since then seen a steady increase in maximum intensity. Modern laser systems are now able to generate ultra-short laser pulses with durations on the order of tens of femtoseconds and focus them down to spots of only a few microns in diameter. Despite containing only a modest amount of energy, typically on the order of 1-100 J, when focused and fully compressed these pulses can reach intensities up to a staggering $10^{21} - 10^{22}\,\mathrm{W/cm^2}$. To fully grasp the sense of these numbers, such intensities are comparable to focusing all sunlight caught by the earth down to a spot with the width of a human hair.

In the interaction of ultra-intense laser fields with matter, be it a solid, liquid or gas, even the leading edge of the laser pulse is intense enough to rapidly ionize the material, despite being much less intense. As a result, the study of these interactions is naturally that of a laser field interacting with a plasma. Consisting of unbound charges, the dynamics of a plasma is generally complex, highly nonlinear and is characterized by collective be-

haviour. In their interaction, the intense laser fields will induce relativistic motion of the charges in the plasma, further complicating the plasma dynamics. Such laser induced plasmas have found uses in studies of warm dense matter, laboratory astrophysics and fusion research. The ability of a plasma to sustain acceleration gradients orders of magnitude larger than those achieved by conventional accelerators has also led to a great interest in laser-driven plasma-based particle acceleration and radiation generation, with applications in materials science, biology and medicine.

Because of the highly nonlinear and complex dynamics involved in intense laser-matter interactions it is difficult to study these systems analytically, often requiring large scale numerical simulations. Plasma simulations can be carried out using several numerical methods, solving the fluid equations for each particle species or the Vlasov-Maxwell equations in the kinetic description. In simulating intense laser-matter interaction it is however more common to use single-particle or *particle-in-cell* (PIC) codes. Because of its effective sampling of phase space and self-consistent treatment of the particle-field system, while being relatively easy to parallelize, the PIC method has become the standard tool for large scale simulations in this field. In this method, the particle distribution functions are sampled in continuous phase space and evolved through the equations of motion of the particles. The fields are solved self-consistently on a discrete computational mesh and evolved through Maxwell's equations, where the source terms are computed as moments of the distribution function. Finally, because of its general simplicity the PIC method allows for substantial modification and extension, which has made it possible to cover an even wider range of regimes, such as effects of strong field QED.

The outline of the thesis is as follows. Chapter 2 gives a brief introduction to plasma theory by presenting basic plasma properties, the governing equations of electromagnetic fields and finally coupling those equations to the main equations describing plasmas. Chapter 3 introduces the particle-in-cell approach and describes how it is used for efficient, large-scale plasma simulations. Chapter 4 presents the basics of intense laser-matter interaction together with some of the most common acceleration schemes. It goes on to discussing the irradiation of microstructured solid targets, as studied in paper I. Chapter 5 introduces the recently proposed laser-driven ion acceleration scheme studied in paper II, CSWA, motivates its use and design and in detail describes how it works. Chapter 6 contains a summary of the papers included in this thesis. Appendix A describes how to analytically define a periodic distribution function, used in for example paper I.

Finally, the reader should note that the system of units used throughout this thesis is that of Gaussian CGS, unless explicitly written otherwise. This includes the two papers covered in this thesis.

Chapter 2

Plasma

A *plasma* is an *ionized gas* and it is often referred to as the fourth state of matter, after *solid*, *liquid* and *gas*, all illustrated in Figure 2.1. Despite this apparently unremarkable position, it is by far the most abundant phase of ordinary matter in the universe. This is not less true in our own solar system in which most of the matter is contained in the sun, which is a gravitationally confined plasma.

Artificially produced plasmas can be found in a large number of applications ranging from plasma displays, rocket ion thrusters, gas-discharge lamps, fusion energy and plasma torches used in for example plasma cutting and plasma arc welding. These plasmas can exhibit a large number of complex phenomena, and have different properties depending on for example density and temperature.

2.1 General properties

The fundamental building blocks of a plasma are *freely moving* and electrically charged particles, usually electrons and (at least partially ionized) ions. These particles are *free* in the sense that they are not atomically bound to each other and the fact that the particles in the plasma are charged gives it properties that are vastly different from that of a gas. The motion of the charged particles gives rise to electromagnetic (EM) fields, and these fields will in turn affect the motion of the particles. As a result, this interplay between the charged particles and the fields leads to a variety of complex collective behaviours, which are defining features of the plasma.

Despite being made up of charged particles the plasma is often *quasi-neutral*, meaning that it is neutral only on a macroscopic scale. This property arises due to the fact that any separation of charge will give rise to a field that, when acting on the surrounding charges, drives the particles in such a way as to cancel the field, and thereby making the plasma quasi-neutral. The characteristic time scale for this to occur is one of the most important

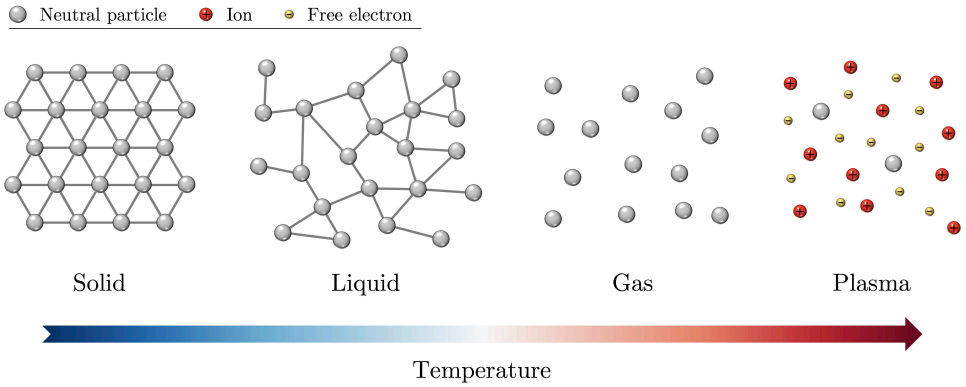

Figure 2.1: Illustration of the four most common states of matter, ordered from left to right by increasing temperature.

parameters of the plasma. For a non-collisional plasma and neglecting the motion of the ions, because of their much larger inertia compared to the electrons, this characteristic time scale can easily be obtained by calculating the oscillation frequency of an electron slab displaced from equilibrium. This frequency is called the (electron) *plasma frequency*, ω_p,

$$\omega_p = \sqrt{\frac{4\pi n_e e^2}{m_e}}, \tag{2.1}$$

where n_e is the unperturbed electron density, e the electron charge and m_e its mass, and it determines the rate at which the plasma responds to local charge density fluctuations.

The tendency of a plasma to cancel out electric fields, and thereby establish quasi-neutrality, can further be described by the fundamental plasma property of *Debye shielding*. Because of this tendency, the electric potential of a test charge located inside the plasma would effectively be screened by the surrounding plasma over some characteristic length scale. This length scale is called the *Debye length* [3] and is, again assuming immobile ions, given by

$$\lambda_D = \sqrt{\frac{k_B T_e}{4\pi n_e e^2}}, \tag{2.2}$$

where k_B is Boltzmann's constant and T_e is the electron temperature. The effective potential of the screened test charge thereby becomes proportional to $\exp(-r/\lambda_D)/r$, decaying exponentially faster than when unscreened. Together, equations (2.1) and (2.2) define the temporal and spatial scales of the interactions in a simple, non-collisional plasma and must be considered when modelling the plasma, in order to correctly capture its collective behaviour.

Studies of plasmas generally look at how a plasma behaves under various conditions or responds to external influence. For the interaction of a plasma

with laser radiation the response of the plasma can be separated into two major regimes, depending on the frequency of the plasma compared to that of the incoming radiation. If the plasma frequency ω_p is smaller than the frequency of the radiation ω_0 then the characteristic time scale of the plasma is longer than the optical period of the incoming radiation. The plasma can therefore not respond quickly enough to stop the propagation of the electromagnetic wave and is thus transparent to it, or *underdense*. In the opposite case, when the plasma frequency is greater than that of the incoming radiation, the characteristic time scale of the plasma is short enough for it to respond to the incoming wave. This response is generally such that it cancels the field in the bulk of the plasma, typically leading to the reflection of the external radiation at the plasma boundary. The plasma thus appear opaque to this radiation and is said to be *overdense*. The natural separation of these two regimes occur when the plasma frequency is equal to that of the incoming radiation and the corresponding *critical density* can, through equation (2.1), be defined as

$$n_{\text{cr}} = \frac{m_e \omega_0^2}{4\pi e^2}. \tag{2.3}$$

Plasmas with densities close to this critical density generally exhibit strong resonance effects in their interaction with the incoming radiation and are typically referred to as *near-critical*.

2.2 Electromagnetic fields

The classical theory of electrodynamics has been one of the most successful areas of not only physics, but science in general, since its birth around the start of the nineteenth century. It rests on *Maxwell's equations*, describing the evolution and generation of electric and magnetic fields by charges and currents, and the *Lorentz force*, describing the force acting upon charged particles by the electric and magnetic fields.

Maxwell's equations read [4]

$$\nabla \cdot \mathbf{E} = 4\pi\rho \tag{2.4}$$

$$\nabla \cdot \mathbf{B} = 0 \tag{2.5}$$

$$\nabla \times \mathbf{E} = -\frac{1}{c}\frac{\partial \mathbf{B}}{\partial t} \tag{2.6}$$

$$\nabla \times \mathbf{B} = \frac{4\pi}{c}\mathbf{J} + \frac{1}{c}\frac{\partial \mathbf{E}}{\partial t} \tag{2.7}$$

where $\mathbf{E}$ and $\mathbf{B}$ are the electric and magnetic fields, $\mathbf{J}$ and ρ are the current and charge densities and c is the speed of light. Separately, equations (2.4), (2.6) and (2.7) are named Coulomb's law (or Gauss' law), Ampère's law and Faraday's law respectively. The remaining equation (2.5) is typically

referred to as the absence of (free) magnetic charge (but occasionally also called Gauss' law for magnetism). Similarly, the Lorentz force is given by

$$\mathbf{F} = q\left(\mathbf{E} + \frac{\mathbf{v}}{c} \times \mathbf{B}\right), \tag{2.8}$$

where $\mathbf{F}$ is the force, due to the electromagnetic fields, acting on a particle of charge q and moving with velocity $\mathbf{v}$.

The electromagnetic fields store energy and the transfer of this energy and transformation into other forms is often of great interest. The energy stored in the fields is described by the electromagnetic energy density

$$u = \frac{1}{8\pi}\left(\mathbf{E}^2 + \mathbf{B}^2\right), \tag{2.9}$$

and the directional flux of electromagnetic energy is similarly given by the *Poynting vector* [5]

$$\mathbf{S} = \frac{c}{4\pi}\mathbf{E} \times \mathbf{B}. \tag{2.10}$$

The electromagnetic energy density and the Poynting vector can further be related through a statement of energy conservation of the electromagnetic fields known as *Poynting's theorem*,

$$\frac{\partial u}{\partial t} + \nabla \cdot \mathbf{S} = -\mathbf{J} \cdot \mathbf{E}, \tag{2.11}$$

which relates the flux of electromagnetic energy to the work done on electric charges.

The total energy content of a localized electromagnetic pulse, at a given instance, can therefore be obtained by simple integration of equation (2.9) over space. While this tells us a global property of the fields, it gives little information about the strength of the fields or the flux of energy. It is therefore often more important to know the *intensity* of the fields, or their *power*. The intensity of the electromagnetic fields is simply the (cycle-averaged) magnitude of the Poynting vector,

$$I = \langle |\mathbf{S}| \rangle, \tag{2.12}$$

describing the flux of energy per unit time and unit area. It can also be defined along a given direction $\hat{\mathbf{n}}$ as $I = \langle \mathbf{S} \cdot \hat{\mathbf{n}} \rangle$. The power of the fields, on the other hand, describe the flux of energy through some surface $\mathcal{S}$ per unit time, and is therefore related to the Poynting vector through integration over this surface,

$$P = \int_{\mathcal{S}} \mathbf{S} \cdot \mathrm{d}\mathbf{A}. \tag{2.13}$$

2.3 Plasma descriptions

There are several ways in which a plasma can be modelled and which description is the most appropriate generally depend on the physical scenario. The most commonly used are the *kinetic* and *fluid* descriptions. These two are usually complemented by the *single-particle* description, in which the interaction between individual particles are neglected. While this description is not technically that of a plasma, it is often used for back-of-the-envelope calculations and can still provide valuable information, especially when dealing with particles in strong background fields.

2.3.1 Kinetic description

In kinetic theory the plasma is described by a set of (single-particle) distribution functions $f_s(\mathbf{r}, \mathbf{v}, t)$ representing the distribution of particles of species s, at position $\mathbf{r}$ and with velocity $\mathbf{v}$. The set of all positions $\mathbf{r}$ and velocities $\mathbf{v}$ (or, alternatively, particle momenta $\mathbf{p}$) is called the *phase space* of the system and is in general six-dimensional. More formally, $f_s(\mathbf{r}, \mathbf{v}, t)$ gives the probability of finding a particle of species s in a neighbourhood of (within the phase space volume $\mathrm{d}^3\mathbf{r}\,\mathrm{d}^3\mathbf{v}$) the phase space point $(\mathbf{r}, \mathbf{v})$, at time t.

The dynamics of such a system can be described by the *Boltzmann equation*

$$\frac{\mathrm{d}f_s}{\mathrm{d}t} = \frac{\partial f_s}{\partial t} + \mathbf{v} \cdot \frac{\partial f_s}{\partial \mathbf{r}} + \frac{\mathbf{F}}{m_s} \cdot \frac{\partial f_s}{\partial \mathbf{v}} = \left(\frac{\partial f_s}{\partial t}\right)_{\mathrm{coll}}, \tag{2.14}$$

where $f_s = f_s(\mathbf{r}, \mathbf{v}, t)$, $\mathbf{F}$ is the force acting upon the particle and m_s is its mass. The right hand side describes the effect of collisions between particles and can be quite complex, requiring additional knowledge of the statistics obeyed by the particles, and can make the Boltzmann equation difficult to solve.

In weakly coupled plasmas where the effect of collisions is small compared to the collective plasma effects, the right hand side of equation (2.14) can be neglected. We thus obtain one of the most important equations in plasma physics, the *Vlasov equation* [6, 7],

$$\frac{\partial f_s(\mathbf{r}, \mathbf{v}, t)}{\partial t} + \mathbf{v} \cdot \frac{\partial f_s(\mathbf{r}, \mathbf{v}, t)}{\partial \mathbf{r}} + \frac{q_s}{m_s}\left(\mathbf{E} + \frac{\mathbf{v}}{c} \times \mathbf{B}\right) \cdot \frac{\partial f_s(\mathbf{r}, \mathbf{v}, t)}{\partial \mathbf{v}} = 0, \tag{2.15}$$

where the Lorentz force from equation (2.8) has now been written out explicitly. The Vlasov equation can be solved self-consistently together with Maxwell's equations, (2.4)–(2.7), where the charge density ρ and current density $\mathbf{J}$ are given by

$$\rho(\mathbf{r}, t) = \sum_s q_s \int f_s(\mathbf{r}, \mathbf{v}, t)\,\mathrm{d}^3\mathbf{v} \tag{2.16}$$

and

$$\mathbf{J}(\mathbf{r},t) = \sum_s q_s \int \mathbf{v} f_s(\mathbf{r},\mathbf{v},t)\,\mathrm{d}^3\mathbf{v}, \tag{2.17}$$

respectively.

2.3.2 Fluid description

In the fluid description the plasma is modelled as a set of interpenetrating fluids, one for each particle species in the plasma, by looking at macroscopic quantities. The fluid equations can be derived from kinetic theory by taking *velocity moments* of the governing kinetic equation (e.g. the Boltzmann or Vlasov equation) and where the n-th moment of f_s can be found by integrating $\mathbf{v}^n f_s$ over velocity space to obtain macroscopic quantities such as the particle number density n_s and mean velocity $\mathbf{v}_s$ of species s. These macroscopic quantities are functions of coordinate space and time, and the fluid description is therefore a simplification of the kinetic description, as the resulting fluid equations are three-dimensional.

Unless truncated by the use of some additional information, taking the moments of the kinetic equation would produce an infinite series of equations. Instead, the moments are closed using a constitutive relation that further ties the moments together, often limiting the number of moment equations to two or three. As an example, integrating the Vlasov equation over all of velocity space gives us the zeroth order moment equation, the *continuity equation*,

$$\frac{\partial n_s}{\partial t} + \nabla \cdot (n_s \mathbf{v_s}) = 0, \tag{2.18}$$

which with the vanishing right-hand side describes that the fluid is conserved, meaning it can neither be created nor destroyed. Instead multiplying the Vlasov equation by $\mathbf{v}$ and again integrating over velocity space gives us the first order moment equation, the *momentum equation*,

$$\frac{\partial \mathbf{v}_s}{\partial t} + (\mathbf{v}_s \cdot \nabla)\mathbf{v}_s = \frac{q_s}{m_s}\left(\mathbf{E} + \frac{\mathbf{v}}{c} \times \mathbf{B}\right) - \frac{\nabla \cdot \mathbf{P}_s}{m_s n_s}, \tag{2.19}$$

where $\mathbf{P}_s$ is the pressure tensor, representing the equation of motion of the fluid of species s. Assuming f_s is isotropic, the last term can be simplified to $\nabla \cdot \mathbf{P}_s = \nabla p_s$ where p_s is the scalar pressure. The fluid equations are then often truncated by for example assuming an adiabatic flow, thus turning the second order moment equation into an *equation of state* for the pressure

$$p_s n_s^{-\gamma_s} = \text{const}, \tag{2.20}$$

where γ_s is the adiabatic index.

So far, we have described each particle species of the plasma in terms of a separate fluid. By making additional assumptions on the particle distribution functions and scale lengths of the plasma, for example being dominated

by collisions, it can instead be modelled as a single fluid. This one-fluid model is also referred to as the *magnetohydrodynamic* (MHD) model and describes the plasma as a single conducting medium, represented by combined macroscopic quantities like the mass density ρ_m, charge density ρ, center-of-mass velocity $\mathbf{V}$, and the electric current density $\mathbf{J}$. The MHD theory is widely used for modelling and describing interstellar plasmas and astrophysical phenomena, magnetically confined fusion plasmas as well as stellar and planetary interiors.

While the fluid description provides a set of equations of reduced dimensionality compared to the kinetic description, making studies of large scale systems more tractable, the simplifications unavoidably also make it restricted in scope. Because the dependence on the velocity distribution is fully neglected, fluid theory can not correctly capture the physics in systems with strong kinetic effects, such as *Landau damping* [8]. In such cases, solving the kinetic equations of kinetic theory is usually the only reliable option.

Chapter 3

Particle-in-cell scheme

Since the equations describing the interaction of plasmas and electromagnetic fields are inherently complex and nonlinear the possibility of studying these systems with analytical tools is very limited. For relativistic plasmas, such as those induced by ultra-intense laser fields, this possibility is reduced even further. This is especially true when considering problems of more dimensions than one, where geometrical considerations can be of great importance. The need for numerical tools for studying these systems should therefore be apparent.

The numerical solution of the Vlasov-Maxwell system of equations provides one of the most detailed description of a collisionless plasma. However, such a simulation would in the general case have to be solved in the fully six-dimensional phase space. Most codes of this type are as a result only employed for studying problems of greatly reduced dimensionality and are therefore restricted in scope. To improve the computational efficiency sophisticated numerical methods such as adaptive mesh refinement can be used, but the implementation of such techniques become increasingly complex for higher dimensions.

Alternatively, plasmas may be studied in the fluid description by solving the fluid equations. This is preferable to solving the kinetic equations when studying large systems as the fluid equations are only three-dimensional. However, the fluid description is a simplification of the kinetic description and can of course only be applied in regimes where its simplifying assumptions are valid. For example, because the dependence of the velocity distribution is lost in the fluid description it becomes inherently unsuitable for the study of systems with strong kinetic effects. This is often the case for plasmas interacting with ultra-intense laser fields.

Instead, the standard tool for large scale relativistic plasma simulations is the particle-in-cell (PIC) scheme [9]. It is a general approach to the numerical solution of partial differential equations such as the Vlasov-Maxwell equations and achieves a much more favourable scaling, than direct solu-

tion of the kinetic equation, by effectively sampling the particle distribution functions. This is done by tracing an ensemble of particles, representing the plasma, in continuous phase space and simultaneously calculating moments of the distribution function on a mesh, representing the simulated coordinate space. The system is advanced in time by self-consistently solving Maxwell's equations for the electromagnetic fields on the mesh as well as the equations of motion for the particles.

3.1 Classical particle-in-cell scheme

At its core the classical PIC method [10] consists of advancing the fields on a computational mesh in the *field solver* and advancing the particles in phase space in the *particle pusher*. In the two intermediate stages the fields are interpolated from the field mesh to the position of the particles and the currents produced by the particles are deposited on the mesh, respectively. The main blocks of the classical PIC method is diagrammatically shown in Figure 3.1. For each iteration, the position and velocity of each particle are used to compute the current density $\mathbf{J}(\mathbf{r})$ using a weighting scheme. This source term is then used in Maxwell's equations in order to advance the electric and magnetic fields $\mathbf{E}$ and $\mathbf{B}$. The charge density $\rho(\mathbf{r})$ can also be calculated, but Coulomb's law (Eq. 2.4) is typically only required as an initial condition. The field values are then interpolated to the position of each particle and the equations of motion are then solved in the particle pusher, where the position and velocity of each particle are updated.

There are several numerical methods which can be employed in the field solver such as FDTD, FEM, and spectral methods, with FDTD being the most commonly used. The mesh is allowed to be very complicated and the individual field components are not required to be co-located, as is the case for the FDTD method in which the mesh is that of a spatially staggered grid known as the *Yee grid* [11]. What is however universal for all of these methods is that the fields are calculated on a discrete mesh.

In the particle pusher the dynamics of the particles are computed according to the Lorentz force (2.8) and similarly to the field solver this can be done in several different ways. The *de facto* standard in plasma physics is the *Boris pusher* [12] in which the particle position and velocity is computed in a leapfrog-like manner and where the latter is most commonly updated in several steps. First, half of the electric impulse is added, then a rotation due to the magnetic field is performed before finally adding the remainder of the electric impulse.

As the physical systems can be very large in terms of the number of particles, with typical number densities of $10^{18}\,\mathrm{cm}^{-3}$ and above, it is often not feasible to simulate the system in its entirety. The workaround used in PIC schemes is to have every simulated particle represent a collection

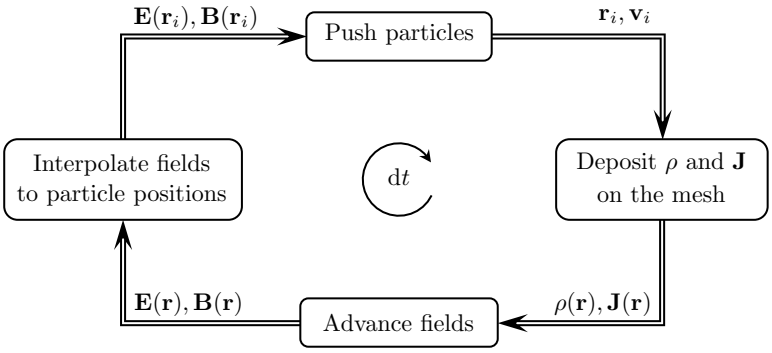

Figure 3.1: Diagrammatic representation of the classical PIC scheme. The vector $\mathbf{r}$ represents grid positions whereas the subscripted vectors, $\mathbf{r}_i$ and $\mathbf{v}_i$, represent positions and velocities of particles.

of real particles of the same type, called a *super-particle*. This is possible because a super-particle in a given field follows a path identical to that of its corresponding real particles, as their charge to mass ratios are the same. Furthermore, the super-particles are treated as being of finite size and are weighted to the mesh according to their shape, or *form factor*. These shapes can most easily be described by B-splines of varying degree, giving an increase in smoothness, but with a trade-off in computational speed. The most commonly used shapes are *nearest grid point* (NGP), *cloud-in-cell* (CIC) and *triangle shaped cloud* (TSC) corresponding to zeroth, first and second order interpolation, respectively. By employing the same weighting scheme for both the current deposition and field interpolation the PIC scheme can be made to conserve momentum. More advanced weighting schemes [13] also exist in order to further guarantee for example charge conservation, but they are in general more computationally intensive.

The PIC approach has proven to be an indispensable tool for advanced studies of plasma dynamics and has turned out to be applicable in a large number of regimes. As it is based on particle dynamics, it is straightforward to relate it to not only classical mechanics, but to quantum mechanical scattering processes as well. This allows the classical PIC scheme to be extended such that it can, to within certain limitations, account for particle collisions [14], ionization [15], radiation reaction [16, 17] and various quantum effects [18–22].

Chapter 4

Laser-plasma interactions

In the following chapter we present basic particle dynamics in intense electromagnetic fields as well as common particle acceleration mechanisms of intense laser-plasma interaction. The main focus of the text is on the question of how laser energy can be transferred to charged particles. In relation to this, we summarize the results of paper I [23], where we study the interaction of an intense laser and a plasma slab with periodic surface structures.

4.1 Single-particle motion in intense fields

Before discussing the interaction of intense laser fields with plasmas it is instructive to first study single-particle dynamics in such fields, as well as define what we actually mean by *intense*. In doing so we will derive some basic properties of importance for the subsequent discussion, following the lines of common textbooks on the topic [4, 24–26].

4.1.1 Non-relativistic motion in a plane wave

We begin by looking at the simple case of a charged particle oscillating non-relativistically in a propagating plane wave field. Assuming that the wave is propagating in the x-direction we may write the electric and magnetic fields as

$$\mathbf{E}(x,t) = E_0\hat{\boldsymbol{\varepsilon}}\mathrm{e}^{i(kx-\omega t)}, \quad \mathbf{B}(x,t) = \hat{\mathbf{x}} \times \mathbf{E}(x,t), \tag{4.1}$$

where E_0 is the field amplitude, ω the frequency, $k = \omega/c$ the wavenumber and $\hat{\boldsymbol{\varepsilon}}$ the polarization vector. The equations of motion for a non-relativistic charged particle under the influence of such fields is simply obtained through the Lorentz force (2.8),

$$m\frac{\mathrm{d}\mathbf{v}}{\mathrm{d}t} = q\left(\mathbf{E}(\mathbf{r},t) + \frac{\mathbf{v}}{c} \times \mathbf{B}(\mathbf{r},t)\right), \quad \frac{\mathrm{d}\mathbf{r}}{\mathrm{d}t} = \mathbf{v}, \tag{4.2}$$

where m and q is the mass and charge of the particle, respectively, and both its position $\mathbf{r}$ and velocity $\mathbf{v}$ are functions of time. For non-relativistic

particle motion the speed of the particle is much smaller than the speed of light, $|\mathbf{v}| \ll c$, and the $\mathbf{v} \times \mathbf{B}$ term can therefore be neglected. The solution to equation (4.2) in this limit is then

$$\mathbf{v} = \frac{iq}{m\omega}\mathbf{E}, \quad \mathbf{r} = -\frac{q}{m\omega^2}\mathbf{E}. \tag{4.3}$$

In order for our assumption of non-relativistic particle motion to hold true we must now require that $|\mathbf{v}| = |q|E_0/m\omega \ll c$, which puts restrictions on the field amplitude E_0. Defining the dimensionless parameter $a_0 = |q|E_0/mc\omega$, our assumption holds true for $a_0 \ll 1$, and particle motion generally becomes relativistic and non-linear for $a_0 \gtrsim 1$, defining what we call the *relativistic regime*. Electrons (and positrons), which have the largest charge-to-mass ratio among the charged particles, will therefore reach this relativistic regime for the lowest field amplitudes. For intense laser pulses this dimensionless parameter is therefore generally defined in terms of the charge and mass of the electron and is called the *normalized laser amplitude*,

$$a_0 = \frac{eE_0}{m_e\omega_0 c}, \tag{4.4}$$

where ω_0 is the laser frequency.

In order to relate the normalized laser amplitude to something more tangible we can further calculate the intensity of the plane wave using equation (2.12). Assuming that the wave is linearly polarized the cycle-averaged intensity is

$$I = \frac{c}{4\pi}\langle|\mathbf{E} \times \mathbf{B}|\rangle = \frac{c}{8\pi}E_0^2 = \frac{c}{8\pi}\left(\frac{m_e\omega_0 c}{e}\right)^2 a_0^2, \tag{4.5}$$

which when rewritten in terms of more common physical units becomes

$$a_0 = 0.85\sqrt{\left(\frac{I}{10^{18}\,\mathrm{W/cm^2}}\right)\left(\frac{\lambda^2}{1\,\mu\mathrm{m}^2}\right)}. \tag{4.6}$$

When speaking of laser fields, the word intense is therefore used to describe the ability to reach the relativistic regime for electrons. Comparing with present state-of-the-art laser systems, capable of reaching $10^{21}\,\mathrm{W/cm^2}$ and with a typical wavelength of $0.81\,\mu\mathrm{m}$, it is currently possible to achieve $a_0 \sim 10$, which is well into the relativistic regime.

4.1.2 Relativistic motion in a plane wave

We now turn to the motion of an electron in an intense field (i.e. in the relativistic regime), in which we can no longer make use of the approximations of the previous section. Instead we set out to derive the exact solution for

arbitrary field intensities. In doing so, instead of working with the electromagnetic fields directly, we will work with the field potentials,

$$\mathbf{B} = \nabla \times \mathbf{A}, \quad \mathbf{E} = -\nabla\phi - \frac{1}{c}\frac{\partial \mathbf{A}}{\partial t}, \tag{4.7}$$

where ϕ and $\mathbf{A}$ is the scalar and vector potential, respectively. Moreover, we will make use of the Lagrangian and Hamiltonian formalisms to derive the constants of motion of the system, instead of directly solving the equations of motion through the Lorentz force.

The Lagrangian L of a relativistic electron in the electromagnetic field, expressed by its potentials, is given by [4, 26–28]

$$L = -mc^2\sqrt{1 - \frac{\mathbf{v}^2}{c^2}} - \frac{e}{c}\mathbf{v}\cdot\mathbf{A} + e\phi. \tag{4.8}$$

We begin by determining the canonical momentum $\tilde{\mathbf{p}}$ of the electron,

$$\tilde{\mathbf{p}} \equiv \frac{\partial L}{\partial \mathbf{v}} = \gamma m\mathbf{v} - \frac{e}{c}\mathbf{A}, \tag{4.9}$$

where $\gamma = (1 - \mathbf{v}^2/c^2)^{-1/2}$ is the Lorentz factor and the first term on the RHS is simply the linear momentum of the electron, $\mathbf{p} = \gamma m\mathbf{v}$. For a propagating monochromatic plane wave the potentials can be expressed as functions of the longitudinal coordinate $r_\parallel$ and time t, and because they obey the wave equation the potentials can be strictly written as functions of the phase $t - r_\parallel/c$. Moreover, because of gauge invariance the potentials can be chosen such that

$$\phi = 0, \quad \nabla\cdot\mathbf{A} = 0, \tag{4.10}$$

and so the plane wave can be fully described by $\mathbf{A} = \mathbf{A}_\perp(t - r_\parallel/c)$ [26]. As a result, the Lagrangian becomes independent of the transverse coordinate $\mathbf{r}_\perp$ ($\partial L/\partial \mathbf{r}_\perp = 0$) and the transverse canonical momentum $\tilde{\mathbf{p}}_\perp$ is therefore conserved ($\mathrm{d}\tilde{\mathbf{p}}_\perp/\mathrm{d}t = 0$).

Another constant of motion can be found for the electron by using the relation $\mathrm{d}H/\mathrm{d}t = -\partial L/\partial t$ between the Hamiltonian and the Lagrangian. The Hamiltonian is given by [27, 28]

$$H(\mathbf{r}, \tilde{\mathbf{p}}, t) \equiv \mathbf{v}\cdot\tilde{\mathbf{p}} - L = \gamma mc^2, \tag{4.11}$$

and describes the energy of the electron. Through the aforementioned relation we obtain

$$\frac{\mathrm{d}H}{\mathrm{d}t} = -\frac{\partial L}{\partial t} = c\frac{\partial L}{\partial r_\parallel} = c\frac{\mathrm{d}}{\mathrm{d}t}\frac{\partial L}{\partial v_\parallel} = c\frac{\mathrm{d}\tilde{p}_\parallel}{\mathrm{d}t}, \tag{4.12}$$

where the second equality comes from the fact that $\mathbf{A}$ is a function of the phase. Our constants of motion can therefore be summarized as

$$\gamma mc - \tilde{p}_{\parallel} = \text{const}, \quad \tilde{\mathbf{p}}_{\perp} = \text{const}. \tag{4.13}$$

If we now wish to proceed, we must first determine these constants from a particular choice of initial conditions. We therefore choose to look at the motion of an electron that in a distant past was at rest ($\mathbf{p} = 0$) and not subject to any field ($\mathbf{A} = 0$). From these conditions, together with equation (4.9) we obtain the linear momentum of the electron

$$p_{\parallel} = (\gamma - 1)mc, \quad \mathbf{p}_{\perp} = \frac{e}{c}\mathbf{A}, \tag{4.14}$$

and using the relativistic energy-momentum relation the momentum components can be shown to be related through

$$p_{\parallel} = \frac{\mathbf{p}_{\perp}^2}{2mc}. \tag{4.15}$$

The equations of motion can therefore be summarized as

$$p_{\parallel} = \frac{1}{2mc}\left(\frac{e}{c}\mathbf{A}\right)^2, \quad \mathbf{p}_{\perp} = \frac{e}{c}\mathbf{A}, \quad \gamma = 1 + \frac{e^2}{2m^2c^4}\mathbf{A}^2. \tag{4.16}$$

Finally, we note that for a plane wave of frequency ω_0 the amplitude of the vector potential A_0 and the amplitude of the field E_0 are related through $E_0 = \omega_0 A_0/c$, (Eq. 4.7). Using this relation, the normalized laser amplitude (Eq. 4.4) can also be expressed as $a_0 = eA_0/m_e c^2$ and is therefore sometimes called the *normalized vector potential*. Thus, after normalizing the vector potential $\mathbf{a} = e\mathbf{A}/m_e c^2$ we finally write down the equations of motion in normalized units

$$\frac{\gamma}{c}\frac{\mathrm{d}r_{\parallel}}{\mathrm{d}t} = \frac{\mathbf{a}^2}{2}, \quad \frac{\gamma}{c}\frac{\mathrm{d}\mathbf{r}_{\perp}}{\mathrm{d}t} = \mathbf{a}, \quad \gamma = 1 + \frac{\mathbf{a}^2}{2}. \tag{4.17}$$

We now solve the equations of motion for a linearly y-polarized plane wave of frequency ω_0 propagating in the x-direction, simply given by the vector potential $\mathbf{a} = (0, a_0, 0)\cos(\omega_0 t - \omega_0 x/c)$. By changing the integration variable to $\tau = t - x/c$, we have

$$\frac{\mathrm{d}\tau}{\mathrm{d}t} = 1 - \frac{v_{\parallel}}{c} = 1 - \frac{p_{\parallel}}{\gamma mc} = 1 - \frac{(\gamma - 1)mc}{\gamma mc} = \frac{1}{\gamma}, \tag{4.18}$$

making equation (4.17) easily solvable. Explicitly, we have that

$$\frac{1}{c}\frac{\mathrm{d}x}{\mathrm{d}\tau} = \frac{a_0^2}{4}\left(1 + \cos 2\omega_0\tau\right), \quad \frac{1}{c}\frac{\mathrm{d}y}{\mathrm{d}\tau} = a_0 \cos\omega_0\tau, \quad \frac{1}{c}\frac{\mathrm{d}z}{\mathrm{d}\tau} = 0, \tag{4.19}$$

which upon integration yields

$$x = \frac{a_0^2}{4}\left(c\tau + \frac{c}{2\omega_0}\sin 2\omega_0\tau\right), \quad y = a_0\frac{c}{\omega_0}\sin\omega_0\tau, \quad z = \text{const.} \tag{4.20}$$

The motion of the electron is thus seen to be composed of two parts, the first of which is a constant drift in the longitudinal direction. From the cycle-averaged motion, the drift velocity v_d is readily obtained to be

$$v_d = \frac{a_0^2}{4 + a_0^2}c. \tag{4.21}$$

This drift is superimposed by a *figure-of-eight* oscillation, as the electron is oscillating with frequency ω_0 in the polarization direction and with frequency $2\omega_0$ in the longitudinal direction. This figure-of-eight motion can be seen in a frame moving in the longitudinal direction with the drift velocity v_d and, by performing an appropriate Lorentz boost to this frame, the corresponding longitudinal motion can be shown to be described by [25]

$$x' = \frac{a_0^2}{8\gamma_0}\frac{c}{\omega_0}\sin 2\omega_0\tau, \tag{4.22}$$

where $\gamma_0 = 1 + a_0^2/4$ and where x' is the longitudinal position in the drift frame.

The electron dynamics described in equations (4.20) and (4.22) are presented in Figure 4.1. Moreover, it is interesting to note that for a circularly polarized plane wave $\mathbf{a} = a_0(0, \cos(\omega_0\tau), \sin(\omega_0\tau))/\sqrt{2}$ the square of the vector potential becomes constant, $\mathbf{a}^2 = a_0^2/2$. Therefore, we have that $\gamma = \gamma_0$ is also constant, making the equations of motion (Eq. 4.17) easily solvable. The resulting electron motion is also presented in Figure 4.1, and is again composed of a constant longitudinal drift with velocity v_d given by equation (4.21). However, there is no longitudinal oscillation in this field and the electron is instead performing a simple circular motion in the transverse plane.

The longitudinal motion of a charged particle in a plane wave field comes from the $\mathbf{v} \times \mathbf{B}$ term of the Lorentz force. However, in spite of this longitudinal motion, and by simply considering the constants of motion, we can see that if the field was to slowly decay over time and eventually vanish, the particle should simply come to a halt. Fortunately, because realistic laser fields are of finite extent and energy, they unavoidably contain spatial gradients which allows for a net energy transfer from the laser field to a particle. Moreover, in the interaction of a laser field with a plasma, the response of the plasma, and the field it generates, is non-negligible and provides further ways of transferring energy. Even so, this simplified treatment provides important insights into charged particle dynamics in intense fields by illuminating several aspects that remain relevant to more complex scenarios.

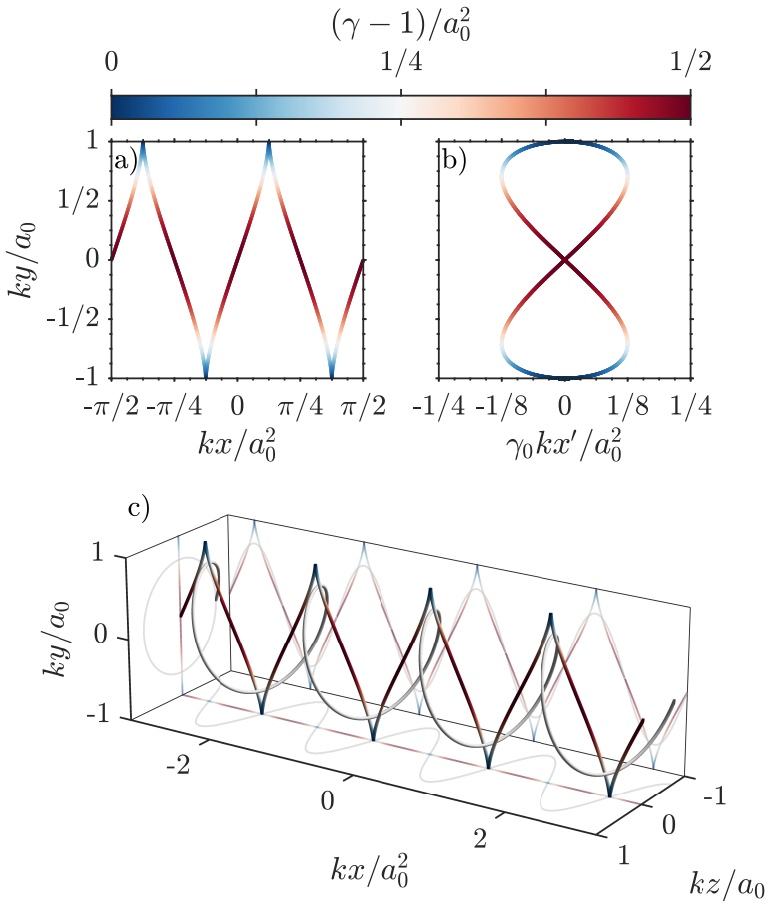

Figure 4.1: The universal trajectory of an electron in a plane wave field of arbitrary intensity. The electron motion in a linearly y-polarized field is presented both: (a, c) in the lab frame and; (b) in the drift frame moving with velocity v_d. (c) Further shows the electron trajectory in a circularly polarized plane wave field. The color scale shows the electron kinetic energy as seen in the lab frame.

4.1.3 Ponderomotive force

A charged particle in an oscillating electromagnetic field will be displaced in the polarization direction by the transverse electric field. If the field is inhomogeneous the displacement of the particle may be to a region of a different field intensity. In such a case, the integrated force in the first and second half of the oscillation cycle will not be equal. As a result the oscillation center of the particle with drift away from regions of higher intensity and toward regions of lower intensity, gaining kinetic energy in the process. This drift motion of the oscillation center can be described by an effective force called the *ponderomotive force*, obtained from the cycle-averaged Lorentz force.

We will here present the standard perturbative derivation of the ponderomotive force, by studying the non-relativistic motion of a charged particle

in an inhomogeneous oscillating field given by

$$\mathbf{E}(\mathbf{r},t) = \mathbf{E}_0(\mathbf{r})\cos\omega_0 t. \tag{4.23}$$

The equation of motion for the particle in this field is the Lorentz force (2.8),

$$m\frac{\mathrm{d}\mathbf{v}}{\mathrm{d}t} = q\left(\mathbf{E}_0(\mathbf{r})\cos\omega_0 t - \frac{\mathbf{v}}{\omega_0}\times[\nabla\times\mathbf{E}_0(\mathbf{r})]\sin\omega_0 t\right), \tag{4.24}$$

where the magnetic field has been obtained through Faraday's law (2.6),

$$\mathbf{B}(\mathbf{r},t) = -\frac{c}{\omega_0}\nabla\times\mathbf{E}_0(\mathbf{r})\sin\omega_0 t. \tag{4.25}$$

First, we separate the motion of the particle into two parts, a slow cycle-averaged motion and a rapid oscillation, described by the vectors $\mathbf{r}_s$ and $\mathbf{r}_r$, respectively. Furthermore, assuming that the spatial variation of the field envelope is small over one oscillation cycle, more strictly expressed as $(\mathbf{v}\cdot\nabla)\mathbf{E}_0 \ll \omega_0\mathbf{E}_0$, the electric field can be expanded around the oscillation center as

$$\mathbf{E}(\mathbf{r},t) = \mathbf{E}(\mathbf{r}_s+\mathbf{r}_r,t) \approx \mathbf{E}(\mathbf{r}_s,t) + (\mathbf{r}_r\cdot\nabla)\mathbf{E}(\mathbf{r}_s,t), \tag{4.26}$$

where we have used that $\mathbf{r} = \mathbf{r}_s + \mathbf{r}_r$. Keeping only the lowest order terms now gives us that

$$m\frac{\mathrm{d}\mathbf{v}_r}{\mathrm{d}t} = q\mathbf{E}_0(\mathbf{r}_s)\cos\omega_0 t, \tag{4.27}$$

where the $\mathbf{v}\times\mathbf{B}$ is left out as it is of first order, because of $|\mathbf{v}| \ll c$. For the rapid oscillatory motion we thus obtain

$$\mathbf{v}_r = \frac{q}{\omega_0 m}\mathbf{E}_0(\mathbf{r}_s)\sin\omega_0 t, \quad \mathbf{r}_r = -\frac{q}{\omega_0^2 m}\mathbf{E}_0(\mathbf{r}_s)\cos\omega_0 t, \tag{4.28}$$

equivalent to equation (4.3).

Next, we turn to the equation of motion for the oscillation center of the particle. By construction we have that $\mathbf{v}_s \ll \mathbf{v}_r$ and to lowest remaining order we obtain the cycle-averaged equation of motion

$$m\left\langle\frac{\mathrm{d}\mathbf{v}_s}{\mathrm{d}t}\right\rangle = -\frac{q^2}{\omega_0^2 m}\left((\mathbf{E}_0\cdot\nabla)\mathbf{E}_0\langle\cos^2\omega_0 t\rangle + \mathbf{E}_0\times(\nabla\times\mathbf{E}_0)\langle\sin^2\omega_0 t\rangle\right), \tag{4.29}$$

where the solutions of equation (4.28) for the rapid motion have been substituted in and where we have written $\mathbf{E}_0 = \mathbf{E}_0(\mathbf{r}_s)$ for brevity. Evaluating the cycle-averages and using the vector relation $\mathbf{E}_0\times(\nabla\times\mathbf{E}_0) = \nabla(\mathbf{E}_0^2)/2 - (\mathbf{E}_0\cdot\nabla)\mathbf{E}_0$, we obtain

$$m\left\langle\frac{\mathrm{d}\mathbf{v}_s}{\mathrm{d}t}\right\rangle = -\frac{q^2}{4\omega_0^2 m}\nabla\mathbf{E}_0^2 \equiv \mathbf{F}_p, \tag{4.30}$$

where the final equality defines the ponderomotive force $\mathbf{F}_p$. The force can be shown to retain this form also for propagating fields and is seen to always point away from regions of higher intensity ($I \sim \mathbf{E}_0^2$) [24, 25]. Interestingly the force can also be seen to be proportional to the square of the charge and inversely proportional to the mass of the particle, as a result affecting charges of opposite sign equally but heavier particles more weakly. For an electron, written in normalized units according to equation (4.4), the force can also be put into the following form

$$\mathbf{F}_p = -m_e c^2 \nabla \frac{\mathbf{a}^2}{4} = -m_e c^2 \nabla \frac{\langle \mathbf{a}^2 \rangle}{2}, \tag{4.31}$$

where $\mathbf{a}$ is the normalized laser amplitude. Finally, we note that the ponderomotive force also can be derived through a completely relativistic treatment [24, 29], but the calculations become much more involved and the details will therefore not be given here.

The ponderomotive force allows for charged particles to gain kinetic energy through interaction with an intense laser field. While its effects, despite its simplicity, are conceptually significant, it is important to remember that the ponderomotive force is merely an effect of the average motion due to the underlying Lorentz force. As such, there are natural limitations to its applicability and since it formally only concerns the motion of the oscillation center, it will naturally be unable to fully capture the particle dynamics.

4.2 Plasma-based acceleration

So far we have only discussed the acceleration of charged particles by intense fields in vacuum. While we have shown such acceleration to be possible, it is often impractical for most applications. The total charge which can be accelerated in such a way is often insufficient and without exact control over parameters such as the laser pulse shape it becomes difficult to accelerate particles into a collimated, monoenergetic beam. Furthermore, because laser fields in vacuum propagate with the speed of light, the particles can not stay perfectly in phase with the field. Together with the fact that intense laser fields in general are very short in duration this limits the total time a particle can spend in this field, in turn severely limiting the total acceleration.

These difficulties can be overcome by instead considering the particles as part of a plasma, in which a laser field can induce collective acceleration through its response to the field. Something very reminiscent of this was proposed as early as 1957 by Veksler [30], in which he envisaged acceleration of charged particles through *coherent motion*. Such "coherent acceleration" is achieved in the many plasma acceleration schemes existing today.

4.2.1 Electron acceleration

Laser-driven plasma-based acceleration of electrons is based on the concept of *laser wakefield acceleration* (LWFA), in which an intense laser pulse is made to propagate through an underdense plasma, typically formed from a gaseous target. As the pulse propagates through the plasma it sets up collective plasma oscillations through which electrons can be accelerated [31, 32].

The most successful variation of LWFA is the so called *bubble regime* [33, 34], in which the ponderomotive push (Eq. 4.30) on the electrons is strong enough to create a cavity, completely evacuated of all electrons. As the electrons are pulled back by the charge separation field this sets up a strong wakefield trailing the evacuated region. The electrons can gain a significant amount of energy through this process and since the group velocity of the laser field in the plasma is lower than the speed of light, phase matching between the accelerated electrons and the laser-driven cavity becomes possible. Furthermore, there are several ways through which electrons can be injected into the cavity and when accelerated in this way have been shown to provide monoenergetic beams of electrons [35, 36]. This has allowed for the acceleration of ultra-short (femtosecond duration) electron bunches to above 1 GeV, over a few centimeters of acceleration distance [37].

4.2.2 Ion acceleration

For laser-driven acceleration of ions, where protons are the lightest and therefore the most mobile, the equations of motion are the same as for the much lighter electrons. However, because of the large difference in mass, $m_p/m_e \sim 1836$, where m_p is the proton mass, we see from the definition of the normalized laser amplitude (Eqs. 4.4 and 4.6) that the intensity of the laser field would have to be more than six orders of magnitude greater in order to induce an equivalent relativistic motion of protons. This implies a lower limit of $10^{24}\,\mathrm{W/cm^2}$ in laser intensity, and for heavier ions the situation gets even more challenging. Furthermore, because ions are much less mobile, the acceleration gradients set up in an underdense plasma by ultra-short laser fields typically fade away well before ions can gain any appreciable amount of energy. This makes ion acceleration by laser wakefields difficult.

This however does not spell the end of laser-driven ion acceleration and there is in fact a whole range of laser-plasma acceleration schemes specifically addressing ion acceleration [38, 39]. Common for most of these schemes is that they concern the interaction of intense laser fields with overdense (or at least near-critical) targets, allowing for the generation of more long-lived acceleration gradients. Furthermore, the ions are generally accelerated *indirectly*, with the energy of the laser field being passed to the ions via the electrons.

The most common ion acceleration schemes include target normal sheath acceleration (TNSA) [40–46], Coulomb explosion (CE) of clusters [47–49], double-layered targets [50–52], hole boring [53], collisionless shock acceleration [54, 55], magnetic vortex acceleration [56, 57] and light sail or radiation pressure acceleration [58–61]. Out of these, the most extensively studied and experimentally accessible scheme is TNSA, wherein a thin foil is illuminated by an intense laser pulse. The electrons in the target are heated by the laser on the illuminated side and then travel through the target to the rear side, where they due to charge separation create an electrostatic acceleration field through which the ions can be accelerated. The scheme gets its name from the fact that the direction of this field is generally normal to the rear surface of the target, where an expanding sheath of plasma containing high-energy ions is formed.

Since the energy of the laser pulse is transferred to the ions in multiple stages, which we in general have little control over, a considerable amount of the total energy is "lost" through a number of side channels. For example, parts of the laser radiation is simply reflected at the plasma-vacuum boundary and because of the transverse motion of the hot electrons, some of the absorbed energy can not be transferred to the ions. As a combined result, this has made TNSA insufficient for a number of potential applications. Considerable efforts have therefore been put into improving upon the shortcomings of the basic scheme. Recently, there have been several studies investigating how microstructures on the target surface can be used to increase the maximum energy of the ions [62–70] as well as improve the collimation of the beam [71, 72]. However, most of these studies focus primarily on how much of the laser energy can be transferred to the target and, by extension, to the ions. Since an absorption of practically 100 % has been shown to be possible this leaves little room for further improvement, and it instead becomes important to more fully understand the dynamics of the intermediaries; the hot electrons.

With this in mind, in paper I [23] we analyse how periodic structures affect the spectral properties of the generated hot electrons, further presented in Figure 4.2. How such structures can be defined analytically, for simulation purposes, is covered in Appendix A. For a flat plasma slab illuminated at an angle θ by an intense laser field and in the absence of surface structures, the angular distribution of the hot electrons follows (see Ref. [23] for details):

$$p_\perp = \frac{\sin\theta}{\cos^2\theta}\left(\sqrt{1+p_\parallel^2\cos^2\theta}-1\right), \tag{4.32}$$

where both the momentum transverse ($p_\perp$) and parallel ($p_\parallel$) to the target normal lies in the plane of incidence. We show that the addition of these structures makes the angular distribution much wider and centers it closer the target normal direction. Furthermore, the increase in absorbed laser energy due to these structures is shown to translate into an increased normal

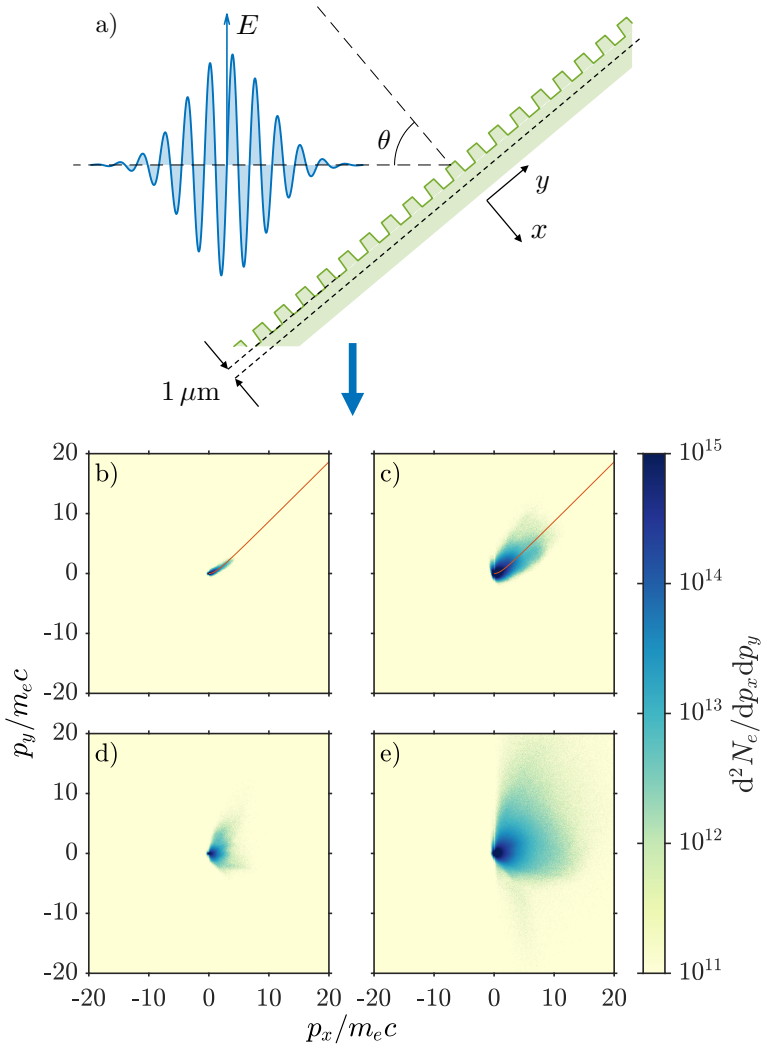

Figure 4.2: (a) The setup consists of a p-polarized Gaussian laser pulse with amplitude $a_0 = 6.3$ and duration $\tau_{\mathrm{FWHM}} = 40\,\mathrm{fs}$, incident on a microstructured, semi-infinite and overdense plasma at an angle to the target normal of θ. A virtual surface (dashed line), at which hot electron distributions are collected, is placed inside the plasma at a distance of $1\,\mu\mathrm{m}$ from the surface, not counting the height of the microstructures. The cumulative momentum space distribution of electrons transiting the virtual surface is shown for: (b, c) a flat foil and; (d, e) a foil with square microstructures with a period equal to the laser wavelength; when irradiated by a laser pulse incident at 45°. The momentum relation predicted by conservation of generalized momenta for an idealized flat foil (Eq. 4.32) is indicated with a red line (b, c). The distributions are shown for two time instances, $t = 225\,\mathrm{fs}$ (b, d) and $t = 500\,\mathrm{fs}$ (c, e). The peak of the pulse reaches the surface at $t = 250\,\mathrm{fs}$.

motion of the electrons. For applications such as TNSA, this potentially reduces the relative energy losses due to transverse electron motion.

Chapter 5

Chirped-standing-wave acceleration

In the following chapter the theoretical basis for the novel acceleration scheme originally proposed in Ref. [73], and further studied in paper II [74] is presented and discussed.

5.1 Motivation

Due to their natural robustness the most experimentally accessible ion acceleration schemes are based on plasma heating as the primary stage in transferring laser energy to the kinetic energy of ions. Despite being experimentally accessible and sufficient for some applications, these schemes have intrinsic limitations that preclude meeting the requirements of more advanced applications. One of the fundamental reasons behind this is a lack of temporal control over the various acceleration stages, thereby providing us with no advanced means for a controlled conversion of laser energy into kinetic energy of ions moving in a chosen direction and with given energy.

The concept of *chirped-standing-wave acceleration* (CSWA) [73] was proposed in an attempt to overcome these difficulties and rests on the idea that in order to control the ion acceleration one must first control the motion of the electrons. This can be achieved by using one or several laser pulses to form a standing wave in which electrons can be trapped. The trapping occurs at the electric field node of the standing wave due to the ponderomotive potential and if this node were to move, the trapped electrons would move with it. Thus, by placing an ultra-thin foil in such a field, the ions in the foil can be accelerated by the charge separation field formed between the electrons and ions as the electrons are continuously displaced by the movement of the node.

This node movement can be achieved in several ways, but the original idea of CSWA was to generate the standing wave using a single laser pulse

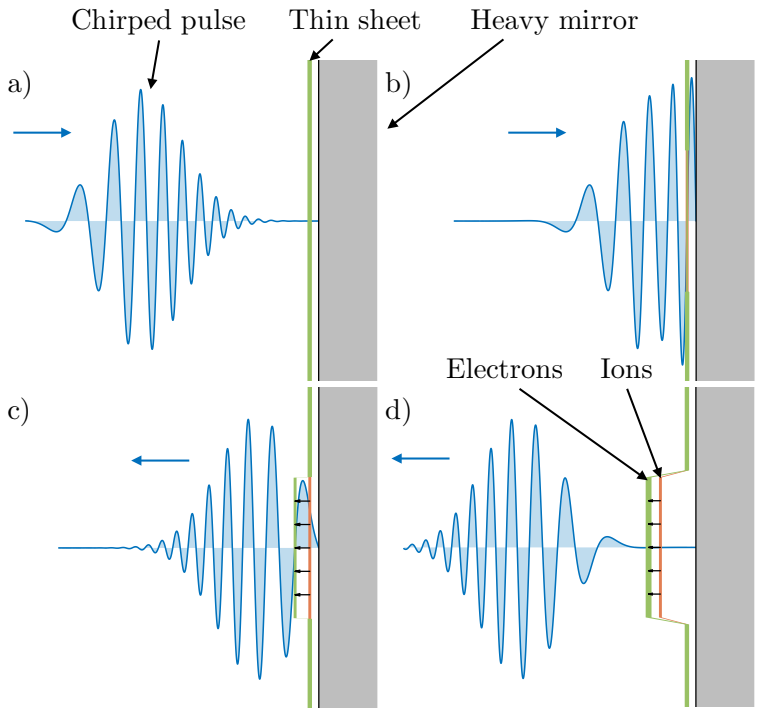

Figure 5.1: Schematic representation of the general scenario of the CSWA concept. (a) A chirped laser pulse incident on a high-density mirror with a thin overdense layer fixed in a position some distance from the mirror. (b) The pulse penetrates the thin layer as it becomes relativistically transparent, forming a standing wave which compresses and locks the electrons to the electric field node. (c) As the frequency of the standing wave decreases the field nodes move away from the mirror and the locked electrons are consequently pulled along, setting up an electrostatic field between them and protons of the thin layer. (d) The electrons are released as the pulse leaves the mirror and the standing wave disappears. The protons, having obtained a significant amount of energy, is travelling away from the mirror.

reflected from a dense mirror, see Figure 5.1. By introducing a chirp to the pulse the position of the node can be made to move with respect to the mirror. Since the frequency is one of the most stable laser parameters, and the chirp of the pulse is relatively easy to control, this results in a tunable acceleration scheme. Furthermore, the locking of the electrons keeps instabilities from forming, which is a major hindrance for many other acceleration schemes. Finally, the laser pulse is circularly polarized in order to drive the electrons in a stable, circular motion. Compared to linear polarization, this restricts the motion of the electrons in the transverse plane, thereby further preventing the formation of instabilities.

5.2 Modelling the chirped laser pulse

Since the chirp of the laser pulse is central to the acceleration scheme, we begin by describing a simple model for a chirped laser pulse with a Gaussian temporal envelope. Assuming that we start out with an unchirped pulse of frequency ω_0, the longitudinal shape can be described by

$$\Psi(\eta) = \psi(\eta)\exp(i\omega_0\eta), \tag{5.1}$$

where the phase is given by $\omega_0\eta = \omega_0(t - x/c)$, and where $\psi(\eta)$ defines the longitudinal envelope. In frequency space, the oscillating term amounts to nothing but a shift of the spectrum

$$\hat{\Psi}(\omega) = \hat{\psi}(\omega - \omega_0), \tag{5.2}$$

where the hat symbolizes the Fourier transform of the function. Describing the envelope as a Gaussian, $\psi(\eta) = \exp(-a\eta^2)$, the frequency spectrum of our pulse is given by

$$\hat{\Psi}(\omega) = \sqrt{\frac{\pi}{a}}\exp\left[-(\omega - \omega_0)^2/4a\right], \tag{5.3}$$

where a can be related to the duration τ_0 of the laser pulse, or alternatively its bandwidth $\Delta\omega$. For laser pulses, these are most commonly expressed in terms of the *full-width at half-maximum* (FWHM) of their intensity

$$a = \frac{2\ln 2}{\tau_0^2}, \quad a = \frac{\Delta\omega^2}{8\ln 2}. \tag{5.4}$$

A chirp can now be introduced by for example passing the pulse through a setup of gratings, similarly to how intense laser pulses can be stretched and recompressed using the chirped-pulse amplification technique. Physically, this introduces a frequency-dependent time delay that alters the relative phase between different frequencies. As an effect, the pulse becomes longer but, more importantly to us, it also obtains a time-variable frequency. To lowest order, this can be achieved with a simple linear chirp, in which the *instantaneous time delay* varies linearly with frequency. Since the instantaneous delay is simply the frequency derivative of the phase, $t_d(\omega) = \mathrm{d}\phi/\mathrm{d}\omega$, the linear chirp is introduced by an additional phase component ϕ, which will have to be quadratic in frequency. Assuming that we also wish to have no time delay of the central frequency we may choose

$$\phi(\omega) = \mathcal{C}(\omega - \omega_0)^2/4a, \tag{5.5}$$

where $\mathcal{C}$ is a *dimensionless chirp parameter*. With this choice, the chirped pulse is simply described by

$$\hat{\Psi}_c(\omega) = \hat{\Psi}(\omega)\exp[-i\phi(\omega)] = \sqrt{\frac{\pi}{a}}\exp\left[-(1 + i\mathcal{C})(\omega - \omega_0)^2/4a\right], \tag{5.6}$$

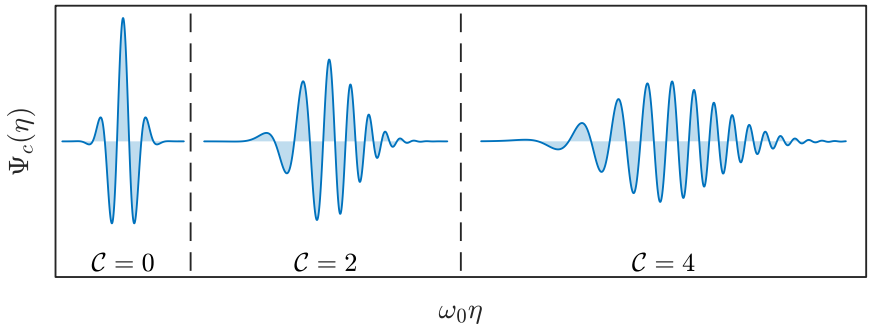

Figure 5.2: Waveform of a Gaussian pulse with bandwidth $\Delta\omega = 0.5\omega_0$, for three different values of the dimensionless chirp parameter $\mathcal{C}$, according to equation (5.7).

and after transforming it back to the time domain it can finally be expressed as

$$\Psi_c(\eta) = \psi_c \exp\left[-\alpha\eta^2 + i(\omega_0\eta + \kappa\eta^2 + \delta)\right], \tag{5.7}$$

where we have defined

$$\psi_c = \frac{1}{\sqrt[4]{1+\mathcal{C}^2}}, \quad \alpha = \frac{1}{1+\mathcal{C}^2}a, \quad \kappa = \frac{\mathcal{C}}{1+\mathcal{C}^2}a, \quad \delta = \frac{\omega_0^2}{4a}\mathcal{C} + \frac{\arctan\mathcal{C}}{2}. \tag{5.8}$$

After studying this expression it can be noted that the constant term in the phase, δ, could have been completely avoided through a different choice of $\phi(\omega)$ in equation (5.5). Furthermore, that the pulse is now linearly chirped can be inferred from the presence of the η^2-term in the phase of equation (5.7), as it allows us to write the instantaneous frequency as a linear function of η,

$$\omega(\eta) = \omega_0 + 2\kappa\eta. \tag{5.9}$$

Finally, the peak amplitude of the pulse is seen to decrease for increasing values of $|\mathcal{C}|$, while the pulse also becomes longer, as expected. The amount of stretching of the pulse is related to the dimensionless chirp parameter as

$$\tau_c/\tau_0 = \sqrt{1+\mathcal{C}^2}, \tag{5.10}$$

where τ_c is the FWHM duration of the chirped pulse. The waveform of an example pulse with bandwidth $\Delta\omega = 0.5\omega_0$ is visualized in Figure 5.2 for different values of chirp.

5.3 Chirped standing wave

By illuminating a dense plasma slab with a laser pulse described by equation (5.7), a chirped standing wave can be formed. For a pulse travelling in the positive x-direction, with the mirror located at $x = 0$, and assuming perfect

reflection, this standing wave will (for $x \leq 0$) be described by two counter-propagating pulses of equal and opposite amplitude. We define $\eta_- = t - x/c$ and $\eta_+ = t + x/c$ for a pulse propagating in the positive and negative x-direction, respectively. By describing the pulse as the real part of equation (5.7) and assuming the intensity gradient to be small, $|\alpha(\eta_+^2 - \eta_-^2)| \ll 1$, the standing wave can be expressed as

$$\Psi_c^{\mathrm{SW}}(x,t) = \Psi_c(\eta_-) - \Psi_c(\eta_+) \approx -2\psi_c \exp(-\alpha\eta_-^2)\sin(A)\sin(B), \quad (5.11)$$

where we have defined

$$A(x,t) = \omega_0 t + \kappa(t^2 + x^2/c^2) + \delta, \quad B(x,t) = (\omega_0 + 2\kappa t)x/c. \quad (5.12)$$

Studying the case of zero chirp, for which $A(x,t) = \omega_0 t$ and $B(x,t) = \omega_0 x/c$, allows us to identify that the argument of the first sine defines the temporal oscillation and the argument of the second defines the node positions of the standing wave. The nodes of the chirped standing wave is therefore given by $B(x,t) = n\pi$, for some integer n, or

$$x = n\frac{\lambda_0}{2}\left(1 + \frac{2\kappa}{\omega_0}t\right)^{-1}, \quad (5.13)$$

where $\lambda_0 = 2\pi c/\omega_0$ is the laser central wavelength. At $t = 0$ the nodes can be seen to be located at half-wavelength steps from the mirror. For $x < 0$ and for the nodes to move *away* from the mirror we further note that a negative chirp is required, $\mathcal{C} < 0$, meaning that the frequency is decreasing (wavelength is increasing) with time. Furthermore, the speed of the node can be obtained through differentiation and shows that higher order nodes (larger $|n|$) will move proportionally faster. It is however important to remember the approximation that $|\alpha(\eta_+^2 - \eta_-^2)| = |4\alpha t x/c| \ll 1$, which restricts the validity for the higher order nodes. In reality such nodes will not be very stable due to beating oscillations.

5.4 Relativistic self-induced transparency

This far we have only considered the formation of the chirped standing wave. However, in order to accelerate ions using this field, we must also be able to place the ions and electrons in one of the nodes. This is achieved through an effect called *relativistic self-induced transparency* (RSIT), by which a plasma becomes transparent to a sufficiently intense laser field. This effect is simply a result of the limiting speed of light, as this also imposes a limit on the current that can be produced by a finite number of charges. For a plasma slab of areal density $\sigma = n_e L$, where L is the thickness of the slab, the maximum possible current is

$$j_{\max} = \sigma c e, \quad (5.14)$$

assuming that only electrons are contributing. Through Faraday's law (2.7) we further obtain that there is a maximum field strength that this current can produce, which would be necessary in order for the plasma slab to reflect the incoming radiation. Assuming circular polarization we get that the threshold intensity that can be reflected by the plasma slab is

$$I_{\mathrm{th}} = \pi c e^2 \sigma^2. \tag{5.15}$$

Further defining the *critical areal density* as $\sigma_{\mathrm{cr}} = \lambda_0 n_{\mathrm{cr}}$, the threshold intensity can be expressed as

$$\frac{I_{\mathrm{th}}}{I_{\mathrm{rel}}} = \pi^2 \left(\frac{\sigma}{\sigma_{\mathrm{cr}}}\right)^2, \tag{5.16}$$

where I_{rel} corresponds to an a_0 of unity.

As we have shown, for a given areal density there is a threshold intensity above which the plasma slab becomes transparent. By placing an ultra-thin foil in front of a mirror we can therefore get the ions and electrons into the standing wave. When irradiated by the intense laser pulse, the thin foil will become relativistically transparent as the intensity surpasses the threshold. Assuming that the mirror is sufficiently dense, the standing wave will then quickly form as the pulse is reflected from the mirror. In order to optimize the acceleration distance of the ions we can therefore place the ultra-thin foil such that its position coincides with the initial position of one of the standing-wave nodes.

5.5 Ion acceleration

As the electrons are displaced by the movement of the electric field nodes of the standing wave, the resulting charge separation will give rise to a micron-sized capacitor-like longitudinal field. Since the maximum strength of this field is proportional to the areal charge density of the thin foil, we want this areal density to be as large as possible, while still allowing for relativistic transparency.

In Ref. [73], these two conditions are considered when estimating the maximum achievable energy of the ions. This is mainly done through an estimate of the total acceleration time of the ions. The study further demonstrates the tunability of the scheme through variation of the chirp, and shows that it is possible to accelerate protons in excess of 100 MeV. Even more importantly, the resulting ion beam is collimated, of high charge and displays a peaked energy spectrum. A typical 2D simulation of proton acceleration using CSWA can be seen in Figure 5.3.

In paper II [74] we discuss *standing-wave acceleration* (SWA) from a more general perspective, not necessarily relying upon chirp to move the

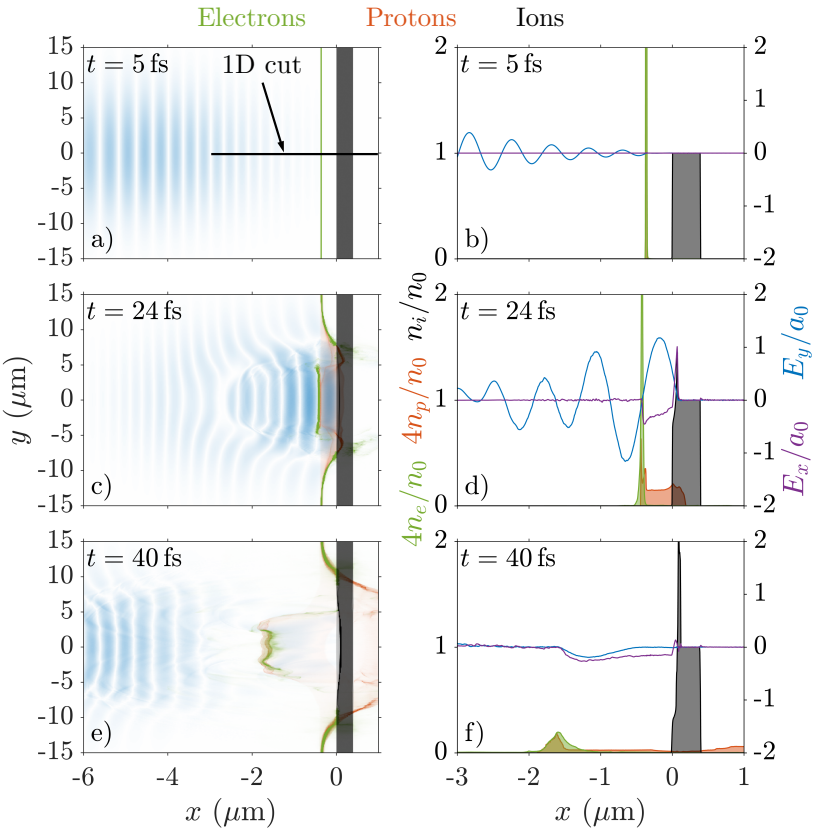

Figure 5.3: A 2D PIC simulation of CSWA for a laser energy $\varepsilon_0 = 80\,\mathrm{J}$, spot size $w = 10\,\mu\mathrm{m}$, bandwidth $\Delta\omega = 0.5\omega_0$ and chirp $\mathcal{C} = -4$ is shown for three time instants: (a, b) before the interaction between the laser pulse and the thin foil; (c, d) during the CSWA stage when the electrons are locked to the standing wave formed by the reflected radiation; (e, f) and some time after the pulse has been reflected and the electrons released. (a, c, e) Magnitude of the transverse electric field E_y (blue), electron density (green), proton density (red), and ion density (grey) as functions of 2D coordinates. (b, d, f) A 1D cut additionally showing the longitudinal electric field E_x (purple) and transverse electric field E_y (blue), with fields obtained for $y = 0$ and densities averaged over the range $|y| < w/2$.

locked electrons. We also demonstrate that CSWA, as a particular implementation of SWA, performs well also under non-ideal conditions and is robust against the effects of limited contrast, misalignment and elliptical polarization. Finally, we discuss the prospects and limitations of CSWA and show that its main limitation lies in the maximum acceleration distance of the ions, which is determined by the bandwidth of the laser pulse. For more details, see Refs. [73, 74].

Chapter 6

Summary of papers

Paper I

Energy partitioning and electron momentum distributions in intense laser-solid interactions

In this paper we demonstrate and assess the effect on the generated hot electrons of adding micro- and nanoscale structures to a plasma slab, illuminated with an intense laser field. We show that the addition of the structures not only increases the absorption of the laser radiation, but also drastically changes the angular distribution of the generated hot electrons.

My contribution to this paper was to develop the numerical diagnostics tools used for tracking the partitioning of energy between different energy channels, perform the simulations and write the paper.

Paper II

Prospects for laser-driven ion acceleration through controlled displacement of electrons by standing waves

In this paper we discuss and elaborate on how controllable laser-driven ion acceleration can be achieved by controlling the electron dynamics using standing waves. We further analyse the robustness of this approach against field structure imperfections, such as those caused by misalignment, elliptical polarization and limited contrast. This is done by focusing on a particular implementation of this approach, Chirped-Standing-Wave Acceleration, and also identify the prospects and limitations of this implementation.

My contribution to this paper was to perform the simulations, obtain the estimates on the laser parameters for when CSWA performs efficiently and write the paper.

Bibliography

[1] T. H. Maiman, Nature **187**, 493 (1960).

[2] D. Strickland and G. Mourou, Opt. Comm. **56**, 219 (1985).

[3] P. Debye and E. Hyckel, Phys. Zeitz. **24**, 185 (1923).

[4] J. D. Jackson, *Classical electrodynamics*, 3rd ed. (Wiley, 1998).

[5] J. H. Poynting, Philos. T. R. Soc. Lond. **175**, 343 (1884).

[6] A. A. Vlasov, J. Exp. Theor. Phys. **8**, 291 (1938).

[7] A. A. Vlasov, J. Phys. USSR **9**, 25 (1945).

[8] L. Landau, J. Phys. U.S.S.R. **10** (1946).

[9] F. Harlow, Los Alamos Scientific Laboratory report LAMS-1956 (1955).

[10] J. M. Dawson, Rev. Mod. Phys. **55**, 403 (1983).

[11] K. Yee, IEEE Trans. Antennas Propag. **14**, 302 (1966).

[12] J. Boris, in *Proc. Fourth Conf. Num. Sim. Plasmas, Naval Res. Lab, Wash. DC* (1970) pp. 3–67.

[13] T. Z. Esirkepov, Comput. Phys. Commun. **135**, 144 (2001).

[14] F. Peano, M. Marti, L. O. Silva, and G. Coppa, Phys. Rev. E **79**, 025701 (2009).

[15] M. Chen, E. Cormier-Michel, C. Geddes, D. Bruhwiler, L. Yu, E. Esarey, C. Schroeder, and W. Leemans, J. Comput. Phys. **236**, 220 (2013).

[16] M. Tamburini, F. Pegoraro, A. D. Piazza, C. H. Keitel, and A. Macchi, New J. Phys. **12**, 123005 (2010).

[17] M. Chen, A. Pukhov, T.-P. Yu, and Z.-M. Sheng, Plasma Phys. Control. Fusion **53**, 014004 (2011).

[18] E. N. Nerush, I. Y. Kostyukov, A. M. Fedotov, N. B. Narozhny, N. V. Elkina, and H. Ruhl, Phys. Rev. Lett. **106**, 035001 (2011).

[19] N. V. Elkina, A. M. Fedotov, I. Y. Kostyukov, M. V. Legkov, N. B. Narozhny, E. N. Nerush, and H. Ruhl, Phys. Rev. ST Accel. Beams **14**, 054401 (2011).

[20] I. V. Sokolov, N. M. Naumova, and J. A. Nees, Phys. Plasmas **18**, 093109 (2011).

[21] C. Ridgers, J. Kirk, R. Duclous, T. Blackburn, C. Brady, K. Bennett, T. Arber, and A. Bell, J. Comput. Phys. **260**, 273 (2014).

[22] A. Gonoskov, S. Bastrakov, E. Efimenko, A. Ilderton, M. Marklund, I. Meyerov, A. Muraviev, A. Sergeev, I. Surmin, and E. Wallin, Phys. Rev. E **92**, 023305 (2015).

[23] J. Magnusson, A. Gonoskov, and M. Marklund, Eur. Phys. J. D **71**, 231 (2017).

[24] P. Mulser and D. Bauer, *High Power Laser-Matter Interaction*, 1st ed., Springer Tracts in Modern Physics 238 (Springer-Verlag Berlin Heidelberg, 2010).

[25] A. Macchi, *A Superintense Laser-Plasma Interaction Theory Primer*, SpringerBriefs in Physics (Springer, 2013).

[26] L. Landau and E. Lifshitz, *The Classical Theory of Fields*, 4th ed. (1975).

[27] A. Fetter and J. Walecka, *Theoretical Mechanics of Particles and Continua*, Dover Books on Physics (Dover Publications, 2003).

[28] H. Goldstein, C. Poole, and J. Safko, *Classical Mechanics*, 3rd ed. (Addison Wesley, 2002).

[29] D. Bauer, P. Mulser, and W. H. Steeb, Phys. Rev. Lett. **75**, 4622 (1995).

[30] V. I. Veksler, Sov. J. At. Energy **2**, 525 (1957).

[31] T. Tajima and J. M. Dawson, Phys. Rev. Lett. **43**, 267 (1979).

[32] C. Joshi, W. B. Mori, T. Katsouleas, J. M. Dawson, J. M. Kindel, and D. W. Forslund, Nature **311**, 525 (1984).

[33] P. Mora and T. M. Antonsen, Phys. Rev. E **53**, R2068 (1996).

[34] A. Pukhov and J. M. ter Vehn, Appl. Phys. B **74**, 355 (2002).

[35] S. P. Mangles, C. Murphy, Z. Najmudin, A. G. R. Thomas, J. Collier, A. E. Dangor, E. Divall, P. Foster, J. Gallacher, C. Hooker, D. A. Jaroszynski, A. J. Langley, W. B. Mori, P. A. Norreys, F. S. Tsung, R. Viskup, B. R. Walton, and K. Krushelnick, Nature **431**, 535 (2004).

[36] J. Faure, Y. Glinec, A. Pukhov, S. Kiselev, S. Gordienko, E. Lefebvre, J.-P. Rousseau, F. Burgy, and V. Malka, Nature **431**, 541 (2004).

[37] W. P. Leemans, B. Nagler, A. J. Gonsalves, C. Tóth, K. Nakamura, C. G. Geddes, E. Esarey, C. Schroeder, and S. Hooker, Nat. Phys. **2**, 696 (2006).

[38] H. Daido, M. Nishiuchi, and A. S. Pirozhkov, Rep. Prog. Phys. **75**, 056401 (2012).

[39] A. Macchi, M. Borghesi, and M. Passoni, Rev. Mod. Phys. **85**, 751 (2013).

[40] S. P. Hatchett, C. G. Brown, T. E. Cowan, E. A. Henry, J. S. Johnson, M. H. Key, J. A. Koch, A. B. Langdon, B. F. Lasinski, R. W. Lee, A. J. Mackinnon, D. M. Pennington, M. D. Perry, T. W. Phillips, M. Roth, T. C. Sangster, M. S. Singh, R. A. Snavely, M. A. Stoyer, S. C. Wilks, and K. Yasuike, Phys. Plasmas **7**, 2076 (2000).

[41] S. C. Wilks, A. B. Langdon, T. E. Cowan, M. Roth, M. Singh, S. Hatchett, M. H. Key, D. Pennington, A. MacKinnon, and R. A. Snavely, Phys. Plasmas **8**, 542 (2001).

[42] A. J. Mackinnon, Y. Sentoku, P. K. Patel, D. W. Price, S. Hatchett, M. H. Key, C. Andersen, R. Snavely, and R. R. Freeman, Phys. Rev. Lett. **88**, 215006 (2002).

[43] M. Roth, A. Blazevic, M. Geissel, T. Schlegel, T. E. Cowan, M. Allen, J.-C. Gauthier, P. Audebert, J. Fuchs, J. Meyer-ter Vehn, M. Hegelich, S. Karsch, and A. Pukhov, Phys. Rev. ST Accel. Beams **5**, 061301 (2002).

[44] P. Mora, Phys. Rev. Lett. **90**, 185002 (2003).

[45] T. E. Cowan, J. Fuchs, H. Ruhl, A. Kemp, P. Audebert, M. Roth, R. Stephens, I. Barton, A. Blazevic, E. Brambrink, J. Cobble, J. Fernández, J.-C. Gauthier, M. Geissel, M. Hegelich, J. Kaae, S. Karsch, G. P. Le Sage, S. Letzring, M. Manclossi, S. Meyroneinc, A. Newkirk, H. Pépin, and N. Renard-LeGalloudec, Phys. Rev. Lett. **92**, 204801 (2004).

[46] M. Passoni, L. Bertagna, and A. Zani, New J. Phys. **12**, 045012 (2010).

[47] T. Ditmire, J. Tisch, E. Springate, M. Mason, N. Hay, R. Smith, J. Marangos, and M. Hutchinson, Nature **386**, 54 (1997).

[48] V. F. Kovalev, V. Y. Bychenkov, and K. Mima, Phys. Plasmas **14**, 103110 (2007).

[49] V. F. Kovalev, K. I. Popov, V. Y. Bychenkov, and W. Rozmus, Phys. Plasmas **14**, 053103 (2007).

[50] T. Esirkepov, S. Bulanov, K. Nishihara, T. Tajima, F. Pegoraro, V. Khoroshkov, K. Mima, H. Daido, Y. Kato, Y. Kitagawa, K. Nagai, and S. Sakabe, Phys. Rev. Lett. **89**, 175003 (2002).

[51] T. Esirkepov, M. Yamagiwa, and T. Tajima, Phys. Rev. Lett. **96**, 105001 (2006).

[52] S. S. Bulanov, A. Brantov, V. Y. Bychenkov, V. Chvykov, G. Kalinchenko, T. Matsuoka, P. Rousseau, S. Reed, V. Yanovsky, D. W. Litzenberg, K. Krushelnick, and A. Maksimchuk, Phys. Rev. E **78**, 026412 (2008).

[53] T. Schlegel, N. Naumova, V. T. Tikhonchuk, C. Labaune, I. V. Sokolov, and G. Mourou, Phys. Plasmas **16**, 083103 (2009).

[54] L. O. Silva, M. Marti, J. R. Davies, R. A. Fonseca, C. Ren, F. S. Tsung, and W. B. Mori, Phys. Rev. Lett. **92**, 015002 (2004).

[55] D. Haberberger, S. Tochitsky, F. Fiuza, C. Gong, R. A. Fonseca, L. O. Silva, W. B. Mori, and C. Joshi, Nat. Phys. **8**, 95 (2012).

[56] S. V. Bulanov, D. V. Dylov, T. Z. Esirkepov, F. F. Kamenets, and D. V. Sokolov, Plasma Physics Reports **31**, 369 (2005).

[57] T. Nakamura, S. V. Bulanov, T. Z. Esirkepov, and M. Kando, Phys. Rev. Lett. **105**, 135002 (2010).

[58] T. Esirkepov, M. Borghesi, S. Bulanov, G. Mourou, and T. Tajima, Phys. Rev. Lett. **92**, 175003 (2004).

[59] A. Henig, S. Steinke, M. Schnürer, T. Sokollik, R. Hörlein, D. Kiefer, D. Jung, J. Schreiber, B. M. Hegelich, X. Q. Yan, J. Meyer-ter Vehn, T. Tajima, P. V. Nickles, W. Sandner, and D. Habs, Phys. Rev. Lett. **103**, 245003 (2009).

[60] S. V. Bulanov, E. Y. Echkina, T. Z. Esirkepov, I. N. Inovenkov, M. Kando, F. Pegoraro, and G. Korn, Phys. Rev. Lett. **104**, 135003 (2010).

[61] S. Kar, K. F. Kakolee, B. Qiao, A. Macchi, M. Cerchez, D. Doria, M. Geissler, P. McKenna, D. Neely, J. Osterholz, R. Prasad, K. Quinn, B. Ramakrishna, G. Sarri, O. Willi, X. Y. Yuan, M. Zepf, and M. Borghesi, Phys. Rev. Lett. **109**, 185006 (2012).

[62] Y. Nodera, S. Kawata, N. Onuma, J. Limpouch, O. Klimo, and T. Kikuchi, Phys. Rev. E **78**, 046401 (2008).

[63] L. Cao, Y. Gu, Z. Zhao, L. Cao, W. Huang, W. Zhou, X. T. He, W. Yu, and M. Y. Yu, Phys. Plasmas **17**, 043103 (2010).

[64] Z. Zhao, L. Cao, L. Cao, J. Wang, W. Huang, W. Jiang, Y. He, Y. Wu, B. Zhu, K. Dong, Y. Ding, B. Zhang, Y. Gu, M. Y. Yu, and X. T. He, Phys. Plasmas **17**, 123108 (2010).

[65] A. Andreev, N. Kumar, K. Platonov, and A. Pukhov, Phys. Plasmas **18**, 103103 (2011).

[66] O. Klimo, J. Psikal, J. Limpouch, J. Proska, F. Novotny, T. Ceccotti, V. Floquet, and S. Kawata, New J. Phys. **13**, 053028 (2011).

[67] D. Margarone, O. Klimo, I. J. Kim, J. Prokůpek, J. Limpouch, T. M. Jeong, T. Mocek, J. Pšikal, H. T. Kim, J. Proška, K. H. Nam, L. Štolcová, I. W. Choi, S. K. Lee, J. H. Sung, T. J. Yu, and G. Korn, Phys. Rev. Lett. **109**, 234801 (2012).

[68] A. Andreev, K. Platonov, J. Braenzel, A. Lübcke, S. Das, H. Messaoudi, R. Grunwald, C. Gray, E. McGlynn, and M. Schnürer, Plasma Phys. Control. Fusion **58**, 014038 (2016).

[69] A. Lübcke, A. A. Andreev, S. Höhm, R. Grunwald, L. Ehrentraut, and M. Schnürer, Sci. Rep. **7**, 44030 (2017).

[70] M. Blanco, M. T. Flores-Arias, C. Ruiz, and M. Vranic, New J. Phys. **19**, 033004 (2017).

[71] L. Giuffrida, K. Svensson, J. Psikal, D. Margarone, P. Lutoslawski, V. Scuderi, G. Milluzzo, J. Kaufman, T. Wiste, M. Dalui, H. Ekerfelt, I. G. Gonzalez, O. Lundh, A. Persson, A. Picciotto, M. Crivellari, A. Bagolini, P. Bellutti, J. Magnusson, A. Gonoskov, L. Klimsa, J. Kopecek, T. Lastovicka, G. A. P. Cirrone, C.-G. Wahlström, and G. Korn, J. Instrum. **12**, C03040 (2017).

[72] L. Giuffrida, K. Svensson, J. Psikal, M. Dalui, H. Ekerfelt, I. Gallardo Gonzalez, O. Lundh, A. Persson, P. Lutoslawski, V. Scuderi, J. Kaufman, T. Wiste, T. Lastovicka, A. Picciotto, A. Bagolini, M. Crivellari, P. Bellutti, G. Milluzzo, G. A. P. Cirrone, J. Magnusson, A. Gonoskov, G. Korn, C.-G. Wahlström, and D. Margarone, Phys. Rev. Accel. Beams **20**, 081301 (2017).

[73] F. Mackenroth, A. Gonoskov, and M. Marklund, Phys. Rev. Lett. **117**, 104801 (2016).

[74] J. Magnusson, F. Mackenroth, A. Gonoskov, and M. Marklund, arXiv:1801.06394.

Appendix A

Periodic structures

As it is common to define target geometries using only analytic expressions, we will here work out how to construct a periodic structure from an arbitrary distribution function, $f(\mathbf{x})$, serving as the unit element to be repeated. This can for example be a function defining the plasma density in some region of phase space.

Since the goal is to repeat some general geometry defined in a limited region of space, we start by identifying how to periodically map a variable onto a closed range. This can be done using a sawtooth function, defined as

$$\text{sawtooth}(x) = x - \lfloor x \rfloor, \tag{A.1}$$

which periodically maps x onto the range $[0, 1]$ and where $\lfloor x \rfloor$ is the floor function. For the more general case, in multiple dimensions and where we only want to repeat the distribution in a subset of the dimensions, we may expand upon this and define the function

$$\mathbf{P}(\mathbf{x}) = \mathbf{x} - P \lfloor \mathbf{x} \rfloor, \tag{A.2}$$

where P is an orthogonal projection matrix, with elements

$$P_{ij}(\mathbf{p}) = \begin{cases} p_i, & i = j \\ 0, & i \neq j \end{cases} \tag{A.3}$$

and where p_i takes on the values 1 or 0 depending on if x_i is repeated or not.

Now, lets say we have an N-dimensional distribution $f(\mathbf{x})$ defined in coordinate system $\mathcal{S}$, which we would like to periodically repeat along a few arbitrary directions. We then assume that the region to be repeated is finite and contained within a unit cell spanned by the vectors $\mathbf{a}_i$, $i = 1, 2, ..., N$. These vectors will now define the directions in which the unit cell may be repeated. Our first course of action is then to transform our distribution

function to the coordinate system $\mathcal{S}'$, in which the unit cell vectors form the basis. We may go between the two systems with the transforms defined by

$$\mathbf{x} = A\mathbf{x}', \quad \mathbf{x}' = A^{-1}\mathbf{x}, \tag{A.4}$$

where

$$A = (\mathbf{a}_1, ..., \mathbf{a}_N). \tag{A.5}$$

In $\mathcal{S}'$ the unit cell is instead contained within the region $x'_i \in [0, 1]$, $i = 1, 2, ..., N$. However, we may further allow for the origin of the unit cell to be placed at $\mathbf{x}_0$, which in the $\mathcal{S}'$ basis is easily obtained from equation (A.4) as

$$\mathbf{x}'_0 = A^{-1}\mathbf{x}_0. \tag{A.6}$$

From equation (A.4) we can also easily obtain the distribution function in the primed coordinate system, $f'(\mathbf{x}')$,

$$f'(\mathbf{x}') = f(A\mathbf{x}'), \tag{A.7}$$

which we will now periodically repeat according to equation (A.2). However, if we wish to place the origin of the unit cell in $\mathbf{x}'_0$ we first note that

$$\mathbf{x} - P\lfloor \mathbf{x} - \mathbf{x}_0 \rfloor = \mathbf{P}(\mathbf{x} - \mathbf{x}_0) + \mathbf{x}_0 \tag{A.8}$$

maps x_i to the range $[x_{0,i}, x_{0,i} + 1]$. Our periodic distribution function in $\mathcal{S}'$ can thus be written

$$f'_p(\mathbf{x}') = f'(\mathbf{P}(\mathbf{x}' - \mathbf{x}'_0) + \mathbf{x}'_0), \tag{A.9}$$

which can be transformed back onto $\mathcal{S}$ using

$$f_p(\mathbf{x}) = f'_p(A^{-1}\mathbf{x}). \tag{A.10}$$

From equations (A.7) through (A.10) we thus obtain the final expression for our periodic distribution function

$$f_p(\mathbf{x}) = f\left(\mathbf{x} - AP\lfloor A^{-1}(\mathbf{x} - \mathbf{x}_0)\rfloor\right). \tag{A.11}$$

The procedure is demonstrated in Figure A.1 for a 2-dimensional distribution function with a shape defined by

$$x^2 + y^2 - r(\varphi) < 0, \quad r(\phi) = 1 - \cos 3\varphi, \quad \tan\varphi = y/x, \tag{A.12}$$

$$\mathbf{a}_1 = L\begin{pmatrix}1\\1\end{pmatrix}, \quad \mathbf{a}_2 = \frac{L}{2}\begin{pmatrix}1\\4\end{pmatrix}, \quad \mathbf{x}_0 = -\frac{L}{2}\begin{pmatrix}1\\2\end{pmatrix}. \tag{A.13}$$

The distribution function is seen to be periodically repeated along the unit cell vectors, however, all features not enclosed by the unit cell have been discarded. It is therefore important to choose an appropriate unit cell in order to reproduce all of the desired features of the original distribution function.

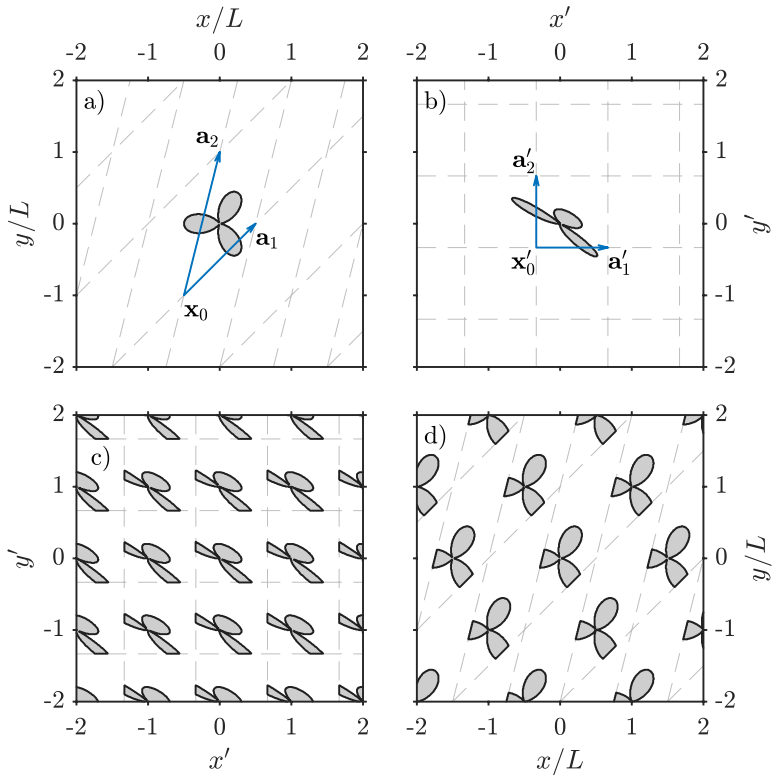

Figure A.1: Demonstration of the steps involved in creating a periodic distribution function. (a) The initial distribution function $f(\mathbf{x})$ with a shape defined by equation (A.12), together with the unit cell defined in equation (A.13). (b) The distribution function $f'(\mathbf{x}')$ in the coordinate space $\mathcal{S}'$, spanned by the unit cell vectors. (c) The periodic distribution function $f'_p(\mathbf{x}')$ in $\mathcal{S}'$. (d) The periodic distribution function $f_p(\mathbf{x})$, transformed back to the original coordinate system $\mathcal{S}$.